Balancing Light Absorptivity and Carrier Conductivity of Graphene Quantum Dots for High-Efficiency Bulk Heterojunction Solar Cells

Jung Kyu Kim,[†,⊥] Myung Jin Park,[‡,⊥] Sang Jin Kim,[‡] Dong Hwan Wang,[†] Sung Pyo Cho,[‡] Sukang Bae,[§,*] Jong Hyeok Park,[†,*] and Byung Hee Hong[‡,*]

[†]SKKU Advanced Institute of Nano Technology (SAINT) and School of Chemical Engineering, Sungkyunkwan University, Suwon 440-746, Republic of Korea, [‡]Department of Chemistry, College of Natural Sciences, Seoul National University, Daehack-doung, Gwanak-gu, Seoul, 151-747, Republic of Korea, and [§]Soft Innovative Materials Research Center, Korea Institute of Science and Technology, Eunha-ri san 101, Bongdong-eup, Wanju-gun, Jeollabukdo (or Jeonbuk) 565-905, Republic of Korea. [⊥]J. K. Kim and M. J. Park contributed equally to this work.

ABSTRACT Graphene quantum dots (GQDs) have been considered as a novel material because their electronic and optoelectronic properties can be tuned by controlling the size and the functional groups of GQDs. Here we report the synthesis of reduction-controlled GQDs and their application to bulk heterojunction (BHJ) solar cells with enhanced power conversion efficiency (PCE). Three different types of GQDs—graphene oxide quantum dots (GOQDs), 5 h reduced GQDs, and 10 h reduced GQDs—were tested in BHJ solar cells, and the results indicate that GQDs play an important role in increasing optical absorptivity and charge carrier extraction of the BHJ solar cells. The enhanced optical absorptivity by rich functional groups in GOQDs increases short-circuit current, while the improved conductivity of reduced GQDs leads to the increase of fill factors. Thus, the reduction level of GQDs needs to be intermediate to balance the absorptivity and conductivity. Indeed, the partially reduced GQDs yielded the outstandingly improved PCE of 7.60% in BHJ devices compared to a reference device without GQDs (6.70%).

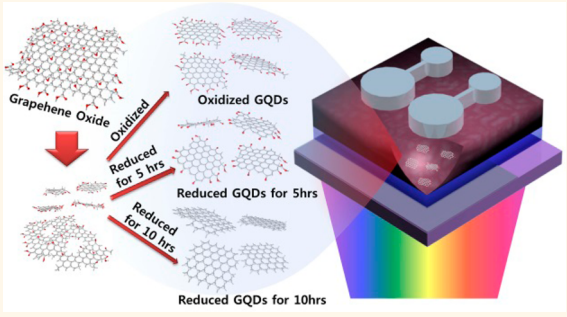

KEYWORDS: graphene quantum dots · bulk heterojunction solar cells · light absorption · conductivity

Organic photovoltaic devices (OPVs) based on bulk heterojunction (BHJ) structure with a blend of polymer donors and fullerene acceptors have been considered as next-generation solar cells due to their possible applications for flexible devices and large-area photovoltaics.[1−5] However, the poor carrier mobility of the BHJ materials usually restricts the thickness of the BHJ film because the recombination of the carriers is directly proportional to the film thickness.[6−8] In recent years, a lot of research has been carried out to improve the power conversion efficiency (PCE) of OPVs with restricted film thickness, exploiting the synthesis of newly designed polymers or small molecules, the modification of morphologies, the plasmon or light scattering using nanopatterned structures, and the novel interlayers as electron or hole conductors.[9−19] Particularly, the addition of metal nanoparticles such as Ag or Au into the OPVs results in considerable improvements in the device performance due to the localized surface plasmon resonances (LSPR) and the incident light scattering or reflection.[20−24] In addition, the device resistance (series or shunt resistance) characteristics can also be improved by mixing the metal nanoparticles in the active layer.[24,25] As alternative approaches, various inorganic nanomaterials including nanoparticles, nanorods, and quantum dots have been exploited as the acceptor materials of the BHJ thin film or hybrid solar cells, improving both the light absorption and the electrical property of the BHJ layers.[26−28] However, these alternative materials are hard to synthesize and usually not environmentally friendly. Moreover, the metal nanoparticles embedded in the BHJ layers often cause a short circuit, leading to permanent damage.

* Address correspondence to lutts@skku.edu (J.H.P.), byunghee@snu.ac.kr (B.H.H), sbae@kist.re.kr (S.B.).

Received for review May 23, 2013 and accepted July 27, 2013.

Published online July 27, 2013
10.1021/nn402606v

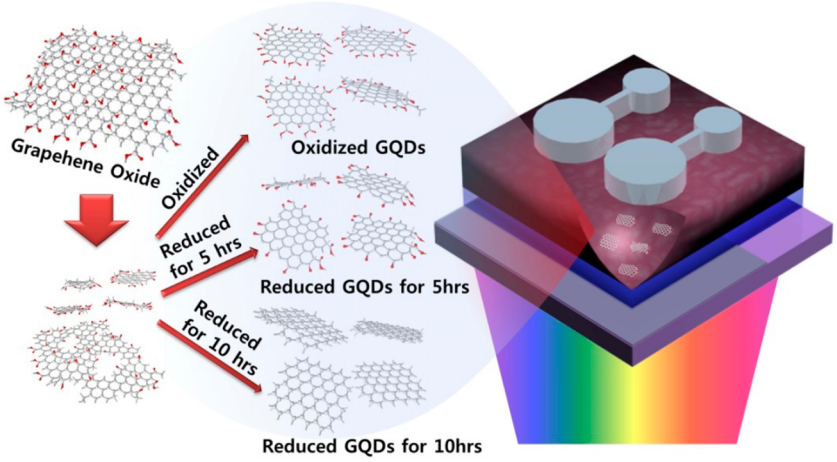

Figure 1. Schematic of a BHJ solar cell with three different types of GQDs, of which edge functional groups are tuned by thermal reduction time.

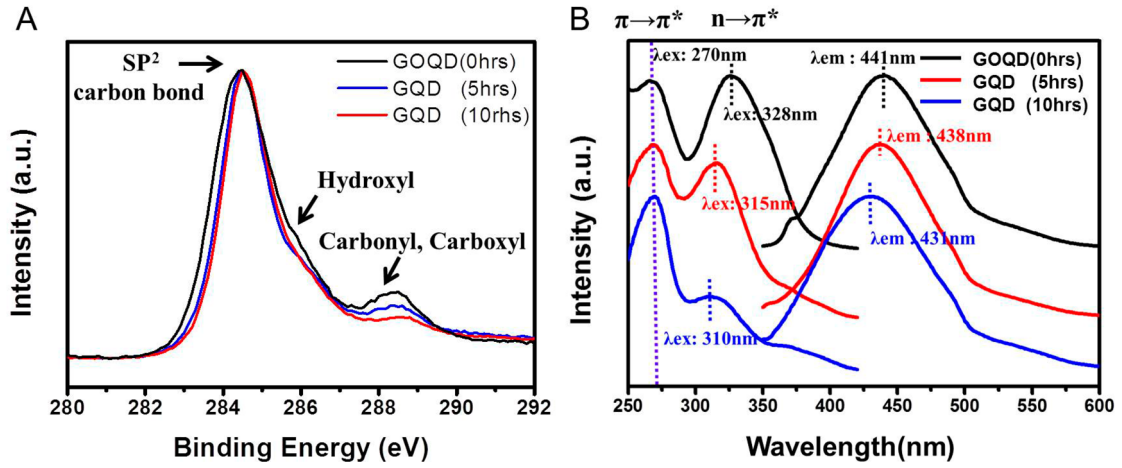

Figure 2. XPS spectra (A) and normalized PLE and PL spectra (B) of GOQD, 5 h reduced GQDs, and 10 h reduced GQD.

Recently, it was reported that a newly emerging material, graphene quantum dots (GQDs), is useful for optoelectronic applications owing to its tunable band gap property depending on size and chemical functionality, which is important to improve the efficiency of optoelectronic devices.[31,32] Moreover, the good dispersity of GQDs in common solvents is expected to enable various solution-processable applications.[33−40] The amount of sp^2 carbon in GQDs can be controlled by varying reduction time, which is useful for optimizing the electrical and optical properties.[35] Thus, we controlled the degree of oxidation while maintaining other parameters constant and found that there is a compromise between short-circuit current (J_{sc}) and fill factors (FF). These values cannot be maximized at the same time, but the optimized reduction condition yields a power conversion efficiency (PCE) superior to a reference device without GQDs.

RESULTS AND DISCUSSION

In this study, we synthesized three different types of GQDs with different oxidation degrees, as shown in Figure 1: oxidized graphene quantum dots (GOQD); 5 h reduced GQDs (GQD 5); and 10 h reduced GQDs (GQD 10). We did not consider further reduction because it tends to saturate after ~10 h. We added the GQDs to the BHJ OPVs with PTB7:PC71BM and found that the positive effect of GQDs varies with the reduction time of GQDs, where J_{sc} increases with oxidation but FF increases with reduction. This indicates that the improved PCE of GQD-embedded OPV devices is relevant to the charge-carrier transportation and the light-absorption ability of the different GQDs. The 5 h reduced GQDs resulted in an increased power conversion efficiency from 6.70% to 7.60%.

GOs possess a large amount of oxygen-based functional groups with sp^2 and sp^3 hybridization.[41,42] In oxidative conditions, the oxygen atoms tend to form a sp^3 bond with carbons by breaking C═C bonds, resulting in sp^3-hybridized epoxy chain structures.[43] Further oxidation leads to the formation of epoxy pairs, carbonyl groups, and hydroxyl groups at the edge sites of GOs.[44] As a result, the size of GOs decreases during the consecutive oxidation processes, while the sp^2−sp^3 carbon ratio is maintained.[45] In the hydrothermal

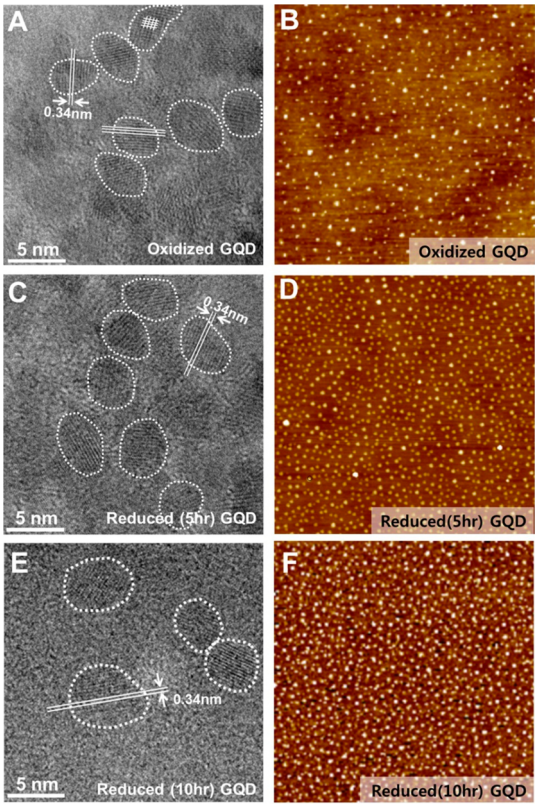

Figure 3. TEM and AFM images of GOQDs (A, B), 5 h reduced GQDs (C, D), and 10 h reduced GQDs (E, F), respectively. The AFM scan ranges are 3 μm $\times$ 3 μm.

reduction process, the oxygen-related functional groups are gradually removed,[35,46] and the three different types of GQDs are prepared by controlling the reduction time. The resulting reduced GQDs show enhanced electrical conductivity as the sp^2 carbon bonds are recovered by reduction.[35,46,48]

The deoxidization of GQDs was investigated by X-ray photoelectron spectroscopy (XPS), Fourier transform infrared spectroscopy (FT-IR), and photoluminescence excitation spectroscopy (PLE). In the C 1s X-ray photoelectron spectra (Figure 2A), the sp^2 carbon peaks at 284.5 eV are almost unchanged, while the hydroxyl carbon peaks at 286.0 eV and the carbonyl/carboxyl peaks at 287.5−288.7 eV decrease with respect to reduction time. We also confirm that the PLE spectrum varies with reduction time, as shown in Figure 2B. Usually, GQD exhibits electronic transition processes similar to benzene that show primary and secondary bands at 202 and 255 nm, respectively.[47] Likewise, GOQD, GQD 5, and GQD 10 show primary excitation bands at ~270 nm and secondary excitation bands at 310, 315, and 328 nm, respectively. The primary band electronic transition at 270 nm approximately corresponds to the energy gap between π and π^* (~1.55 eV), which remains almost constant with increasing reduction time.[48−50] This implies that the GQDs are relatively uniform, as also shown in the TEM and AFM images (Figures 3 and S2). On the contrary, the secondary bands are remarkably different because the amount of

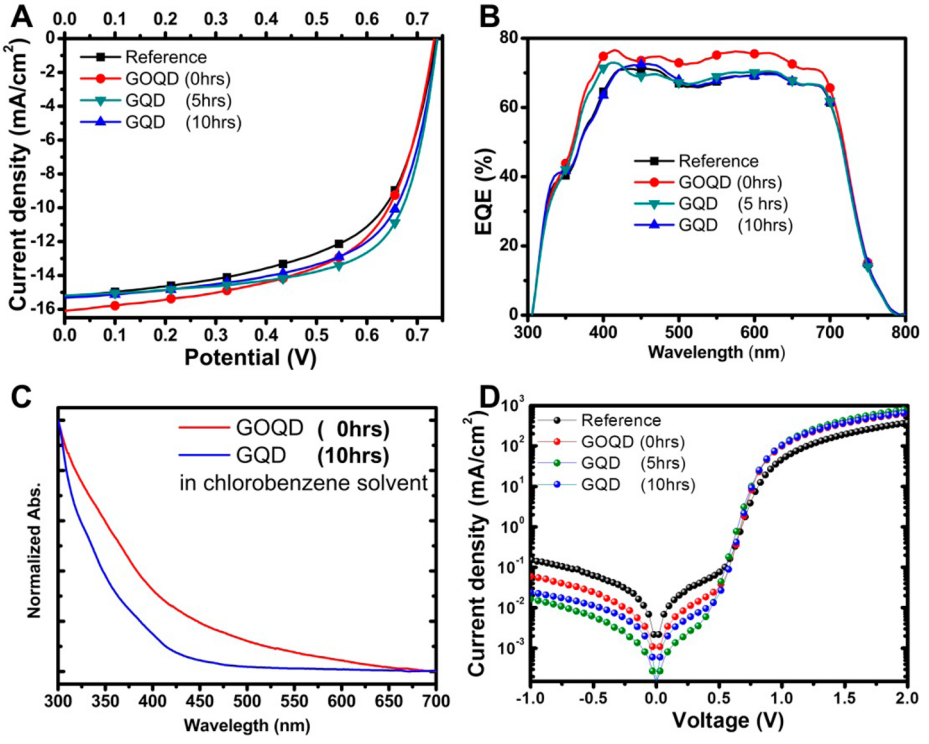

Figure 4. (A) Current *vs* potential (*J*−*V*) curves of the reference and three different GQD-BHJ devices. (B) Incident photon to charge carrier efficiency (IPCE) of the reference and GQD-BHJ devices. (C) UV−visible adsorption spectra of GOQD and GQD 10 in chlorobenzene. (D) Dark *J*−*V* curves of the BHJ devices with no GQDs (black), GOQD (red), GQD 5 (green), and GQD 10 (blue).

oxygen-related functionality responsible for n−π* transition changes with reduction time.[51−53] As a result, the intensity of the secondary excitation band decreases. At the same time, the secondary excitation energy is blue-shifted as the n−π* resonance volume decreases.[51,52] Thus, we conclude that the reduction is unfavorable for the intensity and range of light absorptivity. However, the increase of sp^2 carbons leads to better electrical conductivity, which is advantageous for charge carrier transport.

In order to experimentally verify the positive effects of GQDs in BHJ solar cells, GOQD, GQD 5, and GQD 10 were added in the BHJ layer of PTB7/PC71BM. Figure 3 shows no noticeable size difference between the three different types of GQDs. The GQD content in the BHJ layers was optimized by applying different weight ratios ranging from 0.01 to 0.80 wt %, as shown in Figure S3. The optimized ratio was found to be 0.2 wt % for GOQD, 0.5 wt % for GQD 5, and 0.02 wt % for GQD 10, respectively. The device with a BHJ layer with GOQDs shows the highest J_{sc}, as shown in Figure 4A and Table 1, which is related to the highest incident photon to charge carrier efficiency (IPCE) values of the GOQD device in Figure 4B. This confirms that the functional groups on the edge of GOQD play a positive role in light absorption. The UV−visible absorption spectra of GOQDs and their BHJ device showing a higher absorbance than GQDs also support such positive effects (Figures 4C and S4), which is similar to the case of enhanced absorbance by metal nanoparticles.[23−25] On the other hand, the GQD 5 and GQD 10 devices do not exhibit such noticeable light absorption improvement compared to the reference BHJ device.

However, we found that the fill factors are increased from 59.7% to 67.6% for GQD 5 and to 63.5% for GQD 10, respectively. This implies that the reduction of GQDs plays another positive role in carrier conduction. To investigate the contribution of reduced GQDs to FF, we evaluated series resistances (R_s) and shunt resistances (R_{sh}) in $J-V$ measurements. Due to the small changes in resistance factors, the FF value of the GOQD device was not much improved compared to the reference (Figure 4D and Table 1). However, the $J-V$ characteristics of the partially reduced GQDs (GQD 5) device show clearly increased R_{sh} and FF as well as decreased R_s. This means that the leakage current can be slashed by embedding GQD 5. However, the GQD 10 device shows considerably decreased R_{sh} values and power conversion efficiency, which indicates that the reduction level of GQDs needs to be optimized to maximize the performance of the BHJ solar cells.

TABLE 1. Performance Parameters of the BHJ Devices with No GQDs (reference), GOQD, GQD 5, and GQD 10

device configuration	PCE (%)	FF (%)	J_{sc} (mA/cm^2)	V_{oc} (V)	R_{sh} (KΩcm^2)	R_s (Ωcm^2)
reference	6.70	59.7	15.2	0.738	8.70	2.87
GOQD	7.11	60.4	16.1	0.733	12.82	2.36
GQD 5	7.60	67.6	15.2	0.740	26.60	1.80
GQD 10	7.21	63.6	15.3	0.740	15.20	1.99

CONCLUSION

In summary, we have demonstrated that the OPV performance varies with the degree of reduction in GQDs. By controlling the duration of hydrothermal reduction, strongly oxidized, partially reduced, and strongly reduced GQDs were synthesized. Consequently, we found that the light absorptivity and conductivity of GQDs play different positive roles in enhancing the performance of BHJ OPVs. In the case of GOQDs, the presence of functional groups having nonbonding electrons leads to the resonance effect facilitating the secondary excitation at ∼328 nm. From this property, the device prepared by embedding the GOQDs in the BHJ layer showed a considerable enhancement of absorptivity and thereby an increase of J_{sc}. On the other hand, the excitation band varies with reduction time as the functional groups are removed. When the reduced GQDs were embedded in the BHJ layers, the cell performances reach their optimum point even with relatively lower GQD content compared to the GOQD device. This is possibly due to the enhanced metallic property of reduced GQDs. As a result, the adaption of partially reduced GQDs in OPVs improved the FF from 60.4% to 67.6% and thereby enhanced the PCE from 6.70% to 7.60% by balancing optical absorptivity and electrical conductivity. We believe that this result will provide new insight to solar cell researchers who want to enhance the efficiency of OPVs by utilizing various quantum dot materials. In addition, the further combination of GQD-BHJ solar cells with large-area graphene electrodes on polymer substrates[54,55] would be useful for more enhanced efficiency and flexibility, as demonstrated in organic light-emitting diodes.[56,57]

EXPERIMENTAL SECTION

Synthesis of Oxidized Graphene Quantum Dots. GOs were synthesized by the modified Hummer's method.[58] To make small and uniformly sized RGO powder, the purified GO was subjected to thermal reduction (250 °C, 2 h) inside a box furnace.[45] A 0.5 g amount of reduced GO (RGO) powder was added to the mixture of sulfuric acid and nitric acid and mildly sonicated for 24 h. To remove the acidic ingredients in the solution, the sample was diluted in distilled water after centrifuging for 30 min at 4000 rpm. This rinsing process was repeated six times. The sample was mildly sonicated for 24 h and filtrated through a 0.02 μm nanoporous anodisk. The resulting filtrate was further purified overnight using a 3500 Da dialysis bag.

Synthesis of Reduced Graphene Quantum Dots. The oxidized RGO dispersed in water was placed in small pressure vessel (model no. CV100 II-sin Autoclave) and was subjected to hydrothermal

reduction at 200 °C for 5 and 10 h, respectively. The reduced GQDs were filtered using a 0.02 μm nanoporous anodisk. The brown filtrate was further filtered by a 3500 Da dialysis bag overnight.

Fabrication of OPVs. The BHJ devices composed of PTB7/PC71BM with blended GOQD (oxidized GQDs), GQD 5 (GQDs reduced for 5 h), and GQD 10 (GQDs reduced for 10 h) were prepared. A 40 nm thick hole conducting layer was deposited by spin-casting PEDOT:PSS (AI4083, Clevious) on a precleaned ITO glass and then dried at 150 °C for 15 min. A ~80 nm thick layer of BHJ was spin-coated on top of the PEDOT:PSS layer in an Ar-filled glovebox. The BHJ was prepared to 2.5 wt % in chlorobenzene solution mixed with 3% of 1,8-diiodooctane. The blend ratio of PTB7 (1-Material Chemscitech Inc.) and PC71BM (Nano-c) was 1:1.5 in weight. To optimize the concentration of GQDs in BHJ, GQDs were mixed with the BHJ solution at different weight ratios from 0.01% to 0.80%. Then, a ~6 nm thick TiOx interlayer was spin-coated as an electron conducting layer.[59] Finally, a 100 nm thick Al cathode was thermally evaporated at ~10^{-7} Torr.

Characterization. The FT-IR spectra were obtained by using a Thermo Scientific Nicolet 6700 spectrometer. The AFM images were taken by noncontact mode using a Park System XE-100 atomic force microscope. The TEM images were obtained with a JEOL JEM-3010 electron microscope operating at 200 kV. The absorption and fluorescence spectra were obtained using a Scinco s-3100 spectrophotometer and Jasco FP-8300, respectively. The device performances were measured by Oriel 91193 (1000 W lamp with 100 mW/cm^2 using an NREL-calibrated Si solar cell) and Keithley 2400 source meters. The 5.5 mm^2 aperture was used to determine the cell area.

Conflict of Interest: The authors declare no competing financial interest.

Acknowledgment. This work was supported by the National Core Research Center (NCRC) Program (2011-0006268), the Global Research Lab (GRL) Program (2011-0021972), the Global Frontier Research Program (2011-0031629), and the Basic Science Research Program (2009-0092950, 2012M3A7B4049807, 2011-0017587, 2013K-000165, 2013014038) through the National Research Foundation of Korea (NRF) funded by the Korean government (MEST and MKE).

Supporting Information Available: Additional information on the experimental results can be found in the Supporting Information. This material is available free of charge *via* the Internet at http://pubs.acs.org.

REFERENCES AND NOTES

1. Sariciftci, N. S.; Smilowitz, L.; Heeger, A. J.; Wudl, F. Photoinduced Electron Transfer from a Conducting Polymer to Buckminsterfullerene. *Science* **1992**, *258*, 1474–1476.
2. Yu, G.; Ga, J.; Hummelen, J. C.; Wudl, F.; Heeger, A. J. Polymer Photovoltaic Cells: Enhanced Efficiencies *via* a Network of Internal Donor-Acceptor Heterojunctions. *Science* **1995**, *270*, 1789–1791.
3. Heeger, A. J. Semiconducting and Metallic Polymers: The Fourth Generation of Polymeric Materials. *Angew. Chem., Int. Ed.* **2001**, *40*, 2591–2611.
4. Park, S. H.; Roy, A.; Beaupr, S.; Cho, S.; Coates, N.; Moon, J. S.; Moses, D.; Leclerc, M.; Lee, K.; Heeger, A. J. Bulk Heterojunction Solar Cells with Internal Quantum Efficiency Approaching 100%. *Nat. Photonics* **2009**, *3*, 297–302.
5. Kaltenbrunner, M.; White, M. S.; Głowacki, E. D.; Sekitani, T.; Someya, T.; Sariciftci, N. S.; Bauer, S. Ultrathin and Lightweight Organic Solar Cells with High Flexibility. *Nat. Commun.* **2012**, *3*, 770.
6. Blom, P. W. M.; Mihailetchi, V. D.; Koster, L. J. A.; Markov, D. E. Device Physics of Polymer: Fullerene Bulk Heterojunction Solar Cells. *Adv. Mater.* **2007**, *19*, 1551–1566.
7. Markov, D. E.; Amsterdam, E.; Blom, P. W. M.; Sieval, A. B.; Hummelen, J. C. Accurate Measurement of the Exciton Diffusion Length in a Conjugated Polymer Using a Heterostructure with a Side-Chain Cross-Linked Fullerene Layer. *J. Phys. Chem. A* **2005**, *109*, 5266–5274.
8. Hau, S. K.; Yip, H. L.; Acton, O.; Baek, N. S.; Ma, H.; Jen, A. K. Y. Interfacial Modification to Improve Inverted Polymer Solar Cells. *J. Mater. Chem.* **2008**, *18*, 5113–5119.
9. Wang, D. H.; Moon, J. S.; Seifter, J.; Jo, J.; Park, J. H.; Park, O. O.; Heeger, A. J. Sequential Processing: Control of Nanomorphology in Bulk Heterojunction Solar Cells. *Nano Lett.* **2011**, *11*, 3163–3168.
10. Hoven, C. V.; Dang, X.-D.; Coffin, R. C.; Peet, J.; Nguyen, T.-Q.; Bazan, G. C. Improved Performance of Polymer Bulk Heterojunction Solar Cells Through the Reduction of Phase Separation *via* Solvent Additives. *Adv. Mater.* **2010**, *22*, E63–E66.
11. Ma, W.; Yang, C.; Gonh, X.; Lee, K. H.; Heeger, A. J. Thermally Stable, Efficient Polymer Solar Cells with Nanoscale Control of the Interpenetrating Network Morphology. *Adv. Funct. Mater.* **2005**, *15*, 1617–1622.
12. Brabec, C. J.; Sariciftci, N. S.; Hummelen, J. C. Plastic Solar Cells. *Adv. Funct. Mater.* **2001**, *11*, 15–26.
13. Huo, L.; Hou, J.; Zhang, S.; Chen, H.-Y.; Yang, Y. A Polybenzo-[1,2-*b*:4,5-*b*′]dithiophene Derivative with Deep HOMO Level and Its Application in High-Performance Polymer Solar Cells. *Angew. Chem., Int. Ed.* **2010**, *49*, 1500–1503.
14. Sista, S.; Park, M.-H.; Hong, Z.; Wu, Y.; Hou, J.; Kwan, W. L.; Li, G.; Yang, Y. Highly Efficient Tandem Polymer Photovoltaic Cells. *Adv. Mater.* **2010**, *22*, 380–383.
15. Wang, D. H.; Choi, D. G.; Lee, K. J.; Park, J. H.; Park, O. O. Photovoltaic Devices with an Active Layer from a Stamping Transfer Technique: Single Layer Versus Double Layer. *Langmuir* **2010**, *26*, 9584–9588.
16. Wang, D. H.; Choi, D. G.; Lee, K. J.; Im, S. H.; Park, O. O.; Park, J. H. Unexpected Solid−Solid Intermixing in a Bilayer of Poly(3-hexylthiophene) and [6,6]-phenyl C61-Butyric Acidmethyl Ester *via* Stamping Transfer. *Org. Electron.* **2010**, *11*, 1376–1380.
17. You, J.; Chen, C.-C.; Dou, L.; Murase, S.; Duan, H.-S.; Hawks, S. A.; Xu, T.; Son, H. J.; Yu, L.; Li, G.; Yang, Y. Metal Oxide Nanoparticles as an Electron-Transport Layer in High-Performance and Stable Inverted Polymer Solar Cells. *Adv. Mater.* **2012**, *24*, 5267–5272.
18. Jørgensen, M.; Norrman, K.; Gevorgyan, S. A.; Tromholt, T.; Andreasen, B.; Krebs, F. C. Stability of Polymer Solar Cells. *Adv. Mater.* **2012**, *24*, 580–612.
19. Wang, D. H.; Im, S. H.; Lee, H. K.; Park, O. O.; Park, J. H. Enhanced High-Temperature Long-Term Stability of Polymer Solar Cells with a Thermally Stable TiOx Interlayer. *J. Phys. Chem. C* **2009**, *113*, 17268–17273.
20. Atwater, H. A.; Polman, A. Plasmonics for Improved Photovoltaic Devices. *Nat. Mater.* **2010**, *9*, 205–213.
21. Kim, K.; Carroll, D. L. Roles of Au and Ag Nanoparticles in Efficiency Enhancement of Poly(3-octylthiophene)/C60 Bulk Heterojunction Photovoltaic Devices. *Appl. Phys. Lett.* **2005**, *87*, 203113.
22. Kim, C.-H.; Cha, S.-H.; Kim, S. C.; Song, M.; Lee, J.; Shin, W.; Moon, S.-J.; Bahng, J. H.; Kotov, N. A.; Jin, S.-H. Silver Nanowire Embedded in P3HT:PCBM for High-Efficiency Hybrid Photovoltaic Device Applications. *ACS Nano* **2011**, *5*, 3319–3325.
23. Wang, D. H.; Park, K. H.; Seo, J. H.; Seifter, J.; Jeon, J. H.; Park, J. H.; Park, O. O.; Heeger, A. J. Enhanced Power Conversion Efficiency in PCDTBT/PC70BM Bulk Heterojunction Photovoltaic Devices with Embedded Silver Nanoparticle Clusters. *Adv. Energy Mater.* **2011**, *1*, 766–770.
24. Wang, D. H.; Kim, D. Y.; Choi, K. W.; Seo, J. H.; Im, S. H.; Park, J. H.; Park, O. O.; Heeger, A. J. Enhancement of Donor−Acceptor Polymer Bulk Heterojunction Solar Cell Power Conversion Efficiencies by Addition of Au Nanoparticles. *Angew. Chem., Int. Ed.* **2011**, *50*, 5519–5523.
25. Wang, D. H.; Kim, J. K.; Lim, G.-H.; Park, K. H.; Park, O. O.; Lim, B.; Park, J. H. Enhanced Light Harvesting in Bulk Heterojunction Photovoltaic Devices with Shape-Controlled Ag Nanomaterials: Ag Nanoparticles versus Ag Nanoplates. *RSC Adv.* **2012**, *2*, 7268–7272.
26. Ren, S.; Chang, L.-Y.; Lim, S.-K.; Zhao, J.; Smith, M.; Zhao, N.; Bulovi, V.; Bawendi, M.; Gradecak, S. Inorganic−Organic Hybrid Solar Cell: Bridging Quantum Dots to Conjugated Polymer Nanowires. *Nano Lett.* **2011**, *11*, 3998–4002.
27. Celik, D.; Krueger, M.; Veit, C.; Schleiermacher, H. F.; Zimmermann, B.; Allard, S.; Dumsch, I.; Scherf, U.; Rauscher, F.; Niyamakom, P. Performance Enhancement of CdSe

Nanorod-Polymer Based Hybrid Solar Cells Utilizing a Novel Combination of Post-synthetic Nanoparticle Surface Treatments. *Sol. Energy Mater. Sol. Cells* **2012**, *98*, 433–440.
28. Jeltsch, K. F.; Schädel, M.; Bonekamp, J.-B.; Niyamakom, P.; Rauscher, F.; Lademann, H. W. A.; Dumsch, I.; Allard, S.; Scherf, U.; Meerholz, K. Efficiency Enhanced Hybrid Solar Cells Using a Blend of Quantum Dots and Nanorods. *Adv. Funct. Mater.* **2011**, *22*, 397–404.
29. Huynh, W. U.; Dittmer, J. J.; Alivisatos, A. P. Hybrid Nanorod-Polymer Solar Cells. *Science* **2002**, *295*, 2425–2427.
30. Jaiswal, J. K.; Goldman, E. R.; Mattoussi, H.; Simon, S. M. Use of Quantum Dots for Live Cell Imaging. *Nat. Methods* **2004**, *1*, 73–78.
31. Li, Y.; Hu, Y.; Zhao, Y.; Shi, G.; Deng, L.; Hou, Y.; Qu, L. An Electrochemical Avenue to Green-Luminescent Graphene Quantum Dots as Potential Electron-Acceptors for Photovoltaics. *Adv. Mater.* **2011**, *23*, 776–780.
32. Gupta, V.; Chaudhary, N.; Srivastava, R.; Sharma, G. D.; Bhardwaj, R.; Chand, S. Bottom-Up Fabrication of Photoluminescent Graphene Quantum Dots with Uniform Morphology. *J. Am. Chem. Soc.* **2011**, *133*, 9960–9963.
33. Shen, J.; Zhu, Y.; Yang, X.; Li, C. Graphene Quantum Dots: Emergent Nanolights for Bioimaging, Sensors, Catalysis and Photovoltaic Devices. *Chem. Commun.* **2012**, *48*, 3686–3699.
34. Wang, X.; Zhi, L.; Mullen, K. Transparent, Conductive Graphene Electrodes for Dye-Sensitized Solar Cells. *Nano Lett.* **2008**, *8*, 323–327.
35. Eda, G.; Fanchini, G.; Chhowalla, M. Large-Area Ultrathin Films of Reduced Graphene Oxide as a Transparent and Flexible Electronic Material. *Nat. Nanotechnol.* **2008**, *3*, 270–274.
36. Robinson, J. T.; Perkins, F. K.; Snow, E. S.; Wei, Z.; Sheehan, P. E. Reduced Graphene Oxide Molecular Sensors. *Nano Lett.* **2008**, *8*, 3137–3140.
37. Robinson, J. T.; Zalalutdinov, M.; Baldwin, J. W.; Snow, E. S.; Wei, Z.; Sheehan, P.; Houston, B. H. Wafer-Scale Reduced Graphene Oxide Films for Nanomechanical Devices. *Nano Lett.* **2008**, *8*, 3441–3445.
38. Eda, G.; Lin, Y.-Y.; Miller, S.; Chen, C.-W.; Su, W.-F.; Chhowalla, M. Transparent and Conducting Electrodes for Organic Electronics from Reduced Graphene Oxide. *Appl. Phys. Lett.* **2008**, *92*, 233305.
39. Park, S.; Ruoff, R. S. Chemical Methods for the Production of Graphenes. *Nat. Nanotechnol.* **2009**, *4*, 217–224.
40. Becerill, H. A.; Mao, J.; Liu, Z.; Stoltenberg, R. M.; Bao, Z.; Chen, Y. Evaluation of Solution-Processed Reduced Graphene Oxide Films as Transparent Conductors. *ACS Nano* **2008**, *2*, 463–470.
41. Cai, W.; Piner, R. D.; Stadermann, F. J.; Park, S.; Shaibat, M. A.; Ishii, Y.; Yang, D.; Velamakanni, A.; An, S. J.; Stoller, M.; *et al.* Synthesis and Solid-State NMR Structural Characterization of ^{13}C-Labeled Graphite Oxide. *Science* **2008**, *321*, 1815–1817.
42. Yang, D.; Velamakanni, A.; Bozoklu, G.; Park, S.; Stoller, M.; Piner, R. D.; Stankovich, S.; Jung, I.; Field, D. A.; Ventrice, C. A., Jr.; *et al*. Chemical Analysis of Graphene Oxide Films after Heat and Chemical Treatments by X-Ray Photoelectron and Micro-Raman Spectroscopy. *Carbon* **2009**, *47*, 145–152.
43. Li, J.-L.; Kudin, K. N.; McAllister, M. J.; Prud'homme, R. K.; Aksay, I. A.; Car, R. Oxygen-Driven Unzipping of Graphitic Materials. *Phys. Rev. Lett.* **2006**, *96*, 176101.
44. Li, Z.; Zhang, W.; Luo, Y.; Yang, J.; Hou, J. How Graphene Is Cut upon Oxidation? *J. Am. Chem. Soc.* **2009**, *131*, 6320–6321.
45. Pei, S.; Cheng, H.-M. The Reduction of Graphene Oxide. *Carbon* **2012**, *50*, 3210–3228.
46. Zhou, Y.; Bao, Q.; Tang, L. A. L.; Zhong, Y.; Loh, K. P. Hydrothermal Dehydration for the "Green" Reduction of Exfoliated Graphene Oxide to Graphene and Demonstration of Tunable Optical Limiting Properties. *Chem. Mater.* **2009**, *21*, 2950–2956.
47. Petruska, J. Changes in the Electronic Transitions of Aromatic Hydrocarbons on Chemical Substitution. II. Application of Perturbation Theory to Substituted-Benzene Spectra. *J. Chem. Phys.* **1961**, *34*, 1120.
48. Eda, G.; Lin, Y.-Y.; Mattevi, C.; Yamaguchi, H.; Chen, H.-A.; Chen, I.-S.; Chen, C.-W.; Chhowalla, M. Blue Photoluminescence from Chemically Derived Graphene Oxide. *Adv. Mater.* **2010**, *22*, 505–509.
49. Liu, H.; Ye, T.; Mao, C. Fluorescent Carbon Nanoparticles Derived from Candle Soot. *Angew. Chem., Int. Ed.* **2007**, *46*, 6473–6475.
50. Li, X.; Wang, X.; Zhang, L.; Lee, S.; Dai, H. Chemically Derived, Ultrasmooth Graphene Nanoribbon Semiconductors. *Science* **2008**, *319*, 1229–1232.
51. Closson, W. D.; Haug, P. The Effects of Solvent and Structure on the Low Intensity (n $\rightarrow \pi^*$) Electronic Transition of Carboxylate Esters. *J. Am. Chem. Soc.* **1964**, *86*, 2384–2389.
52. Sidman, J. W. Electronic Transitions Due to Nonbonding Electrons Carbonyl, Aza-Aromatic, and Other Compounds. *Chem. Rev.* **1958**, *58*, 689–713.
53. Luo, Z.; Lu, Y.; Somers, L. A.; Johnson, A. T. C. High Yield Preparation of Macroscopic Graphene Oxide Membranes. *J. Am. Chem. Soc.* **2009**, *131*, 898–899.
54. Kim, K. S.; Zhao, Y.; Jang, H.; Lee, S. Y.; Kim, J. M.; Kim, K. S.; Ahn, J.-H.; Kim, P.; Choi, J.-Y.; Hong, B. H. Large-Scale Pattern Growth of Graphene Films for Stretchable Transparent Electrodes. *Nature* **2009**, *457*, 706–710.
55. Bae, S.; Kim, H.; Lee, Y.; Xu, X.; Park, J.; Zheng, Y.; Balakrishnan, J.; Lei, T.; Kim, H.; Song, Y. I.; *et al.* Roll-to-Roll Production of 30-Inch Graphene Films for Transparent Electrodes. *Nat. Nanotechnol.* **2010**, *5*, 574–578.
56. Han, T.-H.; Lee, Y.; Choi, M.-R.; Woo, S.-H.; Bae, S.-H.; Hong, B. H.; Ahn, J.-H.; Lee, T.-W. Extremely Efficient Flexible Organic Light-Emitting Diodes with Modified Graphene Anode. *Nat. Photonics* **2012**, *6*, 105–110.
57. Ha, J.; Park, S.; Kim, D.; Ryu, J.; Lee, C.; Hong, B. H.; Hong, Y. High-Performance Polymer Light Emitting Diodes with Interface-Engineered Graphene Anodes. *Org. Electron.* **2013**, *14*, 2324–2330.
58. Hirata, M.; Gotou, T.; Horiuchi, S.; Fujiwara, M.; Ohba, M. Thin-Film Particles of Graphite Oxide 1: High-Yield Synthesis and Flexibility of the Particles. *Carbon* **2004**, *42*, 2929–2937.
59. Wang, D. H.; Kim, J. K.; Seo, J. H.; Park, I.; Hong, B. H.; Park, J. H.; Heeger, A. J. Transferable Graphene Oxide by Stamping Nanotechnology: Electron-Transport Layer for Efficient Bulk-Heterojunction Solar Cells. *Angew. Chem., Int. Ed.* **2013**, *52*, 2874–2880.